Graphene-Enabled Superior and Tunable Photomechanical Actuation in Liquid Crystalline Elastomer Nanocomposites

Yingkui Yang, Wenjie Zhan, Rengui Peng, Chengen He, Xinchang Pang, Dean Shi, Tao Jiang, and Zhiqun Lin**

Reconfigurable materials have the propensity to experience the shape and functionality changes in response to the external stimuli and thus convert the electrical, thermal, chemical, and optical energies into mechanical work.[1] The resulting actuators built upon them have a wide range of practical applications in robotics,[2] artificial muscles,[3] switches,[4] motors,[5] and microfluidic devices.[6] However, electrochemical actuators often require a high voltage to generate the movement.[7] Thermomechanical actuators based on phase-transition materials, typically thermotropic liquid-crystalline elastomers (LCEs),[8] are generally limited to their low intrinsic thermal conductivities, thus affording a low energy-transfer ability and slow response to heating. Shape-memory devices produced from alloys and polymers exhibit a one-way response and require a reset after actuation.[9] Moreover, the actuators noted above often involve the complex setup configurations and cannot be operated remotely. In contrast, light-driven actuators employing photodeformable materials carry several advantages, including remote control, convenient manipulation, portability, clean excitation source, electromechanical decoupling, and low noise.[10] Over the past years, photochromic azobenzene-containing LCEs have been primarily used for photoactuators triggered by the trans–cis isomerization upon the alternating ultraviolet (UV) and visible light irradiations.[11] Clearly, such reversible photomechanical actuation requires a switching operation of two light sources at different wavelengths, which are not viable for many practical applications.[12] In addition, the optically initiated actuation is often limited to the UV irradiation and has a slow response (>10 s).[12,13]

Carbon nanotubes (CNTs)[14] and graphene[15] possess strong absorptions in the visible and near-infrared (NIR) regions. They absorb NIR[16] and white lights[17] and rapidly convert photon energy into thermal energy. This unique photothermal effect together with their high thermal conductivity makes CNTs[18] and graphene[19] the efficient nanoheaters to generate localized heating, thereby inducing the conformational change and/or phase transition of the elastomer matrix.[20] Recently, comparing to its counterparts containing graphite oxide, carbon black, and CNTs, graphene was found to impart the higher actuation stress to thermoplastic polydimethylsioxane (PDMS).[21] A larger amplitude of stress response was also observed for monolayer graphene/PDMS in comparison with few-layer graphene/PDMS composites under the comparable loadings.[22] However, graphene sheets are often randomly dispersed in the polymer matrix, providing relatively small deformation, weak actuation, and slow response due to the composition of local vectors driven by each graphene.[23] Moreover, graphene sheets tend to self-aggregate into larger ones and are incompatible with the most polymers, thereby resulting in inhomogeneous composites with a weak interfacial adhesion and thus a low efficiency of load transfer between polymer and graphene.[24] Notably, the homogeneous alignment and binding of graphene sheets into polymers with highly efficient photoactuation has yet to be reported.

Herein, we report a robust strategy for the in situ crafting of reversibly photodeformable graphene/LCE nanocomposites possessing superior and tunable photomechanical actuation properties upon the exposure to NIR irradiation. These graphene-containing LCE nanocomposites were judiciously yielded by combining the in situ UV photopolymerization of liquid-crystal monomers (LCMs) with the concurrent hot-stretching process. In this NIR-actuated system, graphene sheets play an important role of being photoactive constituent. The laterally attached aromatic mesogens of LCMs ensure the formation of stable suspension of graphene sheets and, subsequently, their uniform dispersion in the LCE matrix through the π–π stacking between LC aromatic rings and graphene, and the hydrogen bonding between the hydroxyl and carboxyl groups in graphene and the ester groups in LCMs and the resulting LCEs. It is noteworthy that the self-orientation of LC in conjunction with the hot-drawing process synergistically renders graphene to be highly aligned in the LCE matrix. To the best of our knowledge, there have been no reports on the creation of aligned graphene/LCE nanocomposites for photomechanical actuation. The LCEs exhibit two distinct advantages, that is, the self-organization nature of LCs and the entropy-driven elasticity that enables the larger reversible deformations compared to conventional polymeric materials.[25] More importantly, the photoresponsive parameters including deformation amplitude, actuation stress and response rate can be rationally controlled by tailoring the sp^2-hybridized carbon of graphene, its loading content and

Prof. Y. Yang, W. Zhan, R. Peng, C. He,
Prof. D. Shi, Prof. T. Jiang
MOE Key Laboratory for Green Preparation
and Application of Functional Materials
Hubei Collaborative Innovation Center for
Advanced Organic Chemical Materials
and School of Materials Science and Engineering
Hubei University
Wuhan 430062, China
E-mail: ykyang@hubu.edu.cn
Prof. Y. Yang, Dr. X. Pang, Prof. Z. Lin
School of Materials Science and Engineering
Georgia Institute of Technology
Atlanta, GA 30332, USA
E-mail: zhiqun.lin@mse.gatech.edu

DOI: 10.1002/adma.201503680

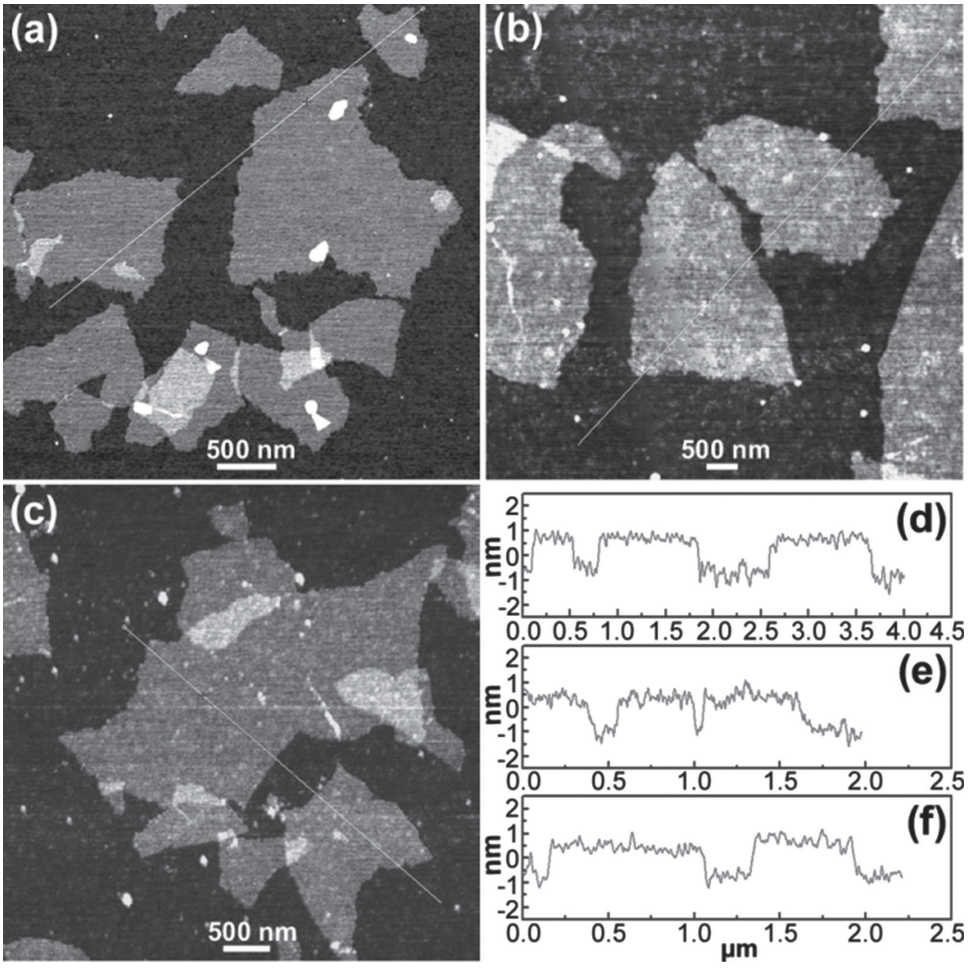

Figure 1. AFM images of a) GO, b) LRGO, and c) HRGO sheets and their corresponding height profiles d–f) along the white lines shown in (a–c), i.e., d) for a), e) for b), and f) for c).

its alignment in LCEs. Remarkably, large strain (35.7%), high mechanical force (240 kPa), high initial sensitivity (<0.5 s), fast reversible photoresponse (≈8 s), and long-term cyclability were collectively achieved in graphene/LCE nancomposites composed of aligned graphene with a large fraction of sp^2-bonded carbons.

Graphene sheets with different sp^2-hybridized carbons were first prepared by the solvothermal reduction of graphene oxide (GO) in *N*-methyl-2-pyrrolidinone (NMP) at low (150 °C) and high (210 °C) temperatures, hereafter referred to as LRGO and HRGO, respectively (see the Supporting Information). The average height of GO sheets was measured by atomic force microscopy (AFM) to be ≈0.98 nm (**Figure 1**a), corresponding to a monolayer-thick sheet.[26] The decreased heights of ≈0.85 nm for LRGO (Figure 1b) and ≈0.82 nm for HRGO (Figure 1c) are due to the deoxygenation of GO on its basal planes.

Figure 2a compares the Raman characteristics of G and D bands appeared at ≈1590 and ≈1320 cm^{-1}, respectively, for GO, LRGO and HRGO. Comparing to GO, the G band of reduced GO shows a redshift of ≈5 cm^{-1}, which is closer to that of graphite, due to the restoration of graphitic sp^2 network after reduction. The integrated intensity ratio of D to G band increases from 1.35 for GO to 1.47 for LRGO and 1.52 for HRGO. This can be attributed to the decrease in the average size of sp^2 aromatic domains from the reduced GO by creating numerous new graphitic domains.[27]

The C 1s spectra of GO, LRGO, and HRGO exhibiting two main peaks in the range of 281–292 eV are shown in Figure 2b. The peaks centered at 284.6 eV correspond to the sp^2-hybridized carbons, while the bands at 285–292 eV can be assigned to the sp^3-bonded carbons originated from the epoxy, hydroxyl, carbonyl, and carboxyl groups.[27a] The fraction of sp^2 bonds within GO is 37.8%, which increases to 55.3% for LRGO and further rises up to 66.3% for HRGO as a result of the restoration of more sp^3 bonds into sp^2 hybridization at the elevated temperature.[28]

Two monomers, namely, LCM-A and LCM-B, were synthesized (see Figure S1 in the Supporting Information). The chemical structures of commercially available cross-linkers of RM-82 and 1,6-hexanediol diacrylate (HODA) and photoinitiator Irgacure 369 are shown in **Figure 3**a; and they were used as received. The solvothermally produced LRGO and HRGO sheets in NMP can form relatively stable colloidal dispersions.[29] The laterally attached mesogenic groups in LCMs

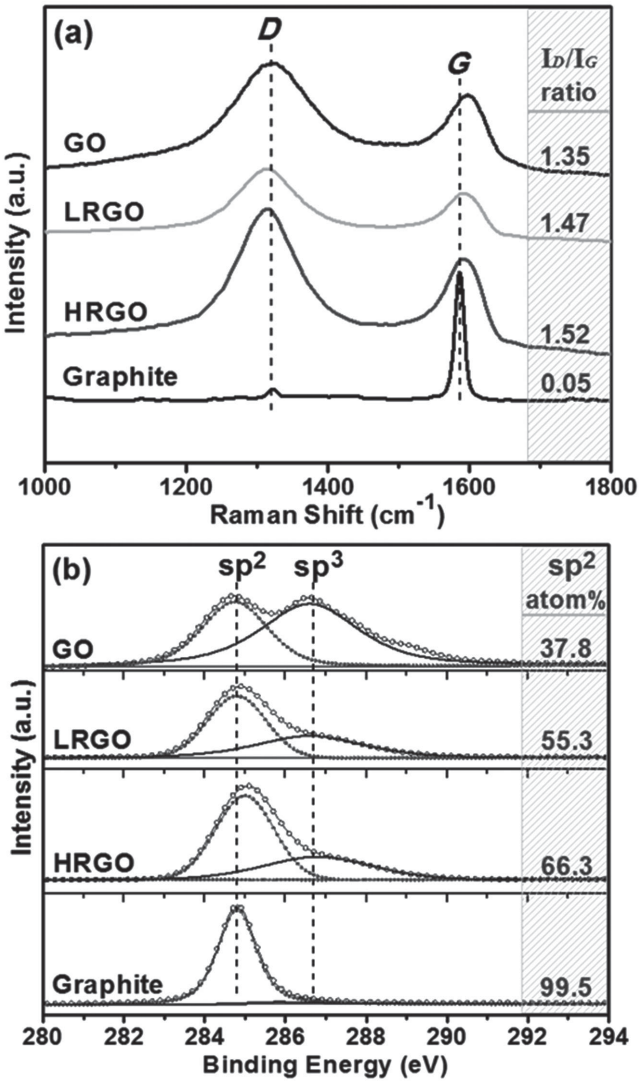

Figure 2. a) Raman spectra (excited at 785 nm) and b) C1s core-level X-ray photoelectron spectroscopy (XPS) spectra of GO, LRGO, HRGO, and graphite, respectively.

enable the formation of macroscopically stable suspensions (Figure S2, Supporting Information) through the effective π–π stacking between LC aromatic rings and graphene, and the hydrogen bonding between the hydroxyl and carboxyl groups in GO and graphene (i.e., both LRGO and HRGO; possessing residual oxygen-containing functional groups) and the ester groups in LCMs. It is important to note that the high dispersion capability and good compatibility of LCMs with GO and graphene impart the successful crafting of homogeneous graphene/LCE nanocomposites via the in situ UV photopolymerization (see the Supporting Information). No phase separation was observed for graphene/LCE nanocomposites, and two transition temperatures corresponding to the glass transition (T_g = 18–25 °C) and the nematic-to-isotropic transition (T_{NI} = 80–86 °C) were seen (Figure S3, Supporting Information). They are lower than those of pure LCEs (i.e., 25.1 and 96.5 °C, respectively) due to the thermal stress of GO and graphene that promotes the phase transition of the LCE matrix.[17,18,30] A similar trend for T_g and T_{NI} for CNT/LCE nanocomposites has been reported.[17,30,31] The much lowered T_{NI} is expected to benefit the fast photomechanical actuation of graphene/LCE nanocomposites.

The pure LCEs before and after the hot-drawing process displayed birefringent textures under the crossed polarizers, signifying the formation of a nematic phase (Figure S4a,b, Supporting Information).[32] The graphene/LCE nanocomposites appeared nearly dark (Figure S4c,d, Supporting Information) due to the blocking of light by graphene sheets.[30] However, upon the rotation of the hot-drawn HRGO/LCE sample to about 45° with respect to polarizer (analyzer), the birefringence stripes were seen due to the stretch-induced alignment of LC mesogens. The aligned stripes along the stretching direction are clearly observed on the surface of nanocomposites, as evidenced by scanning electron microscope (SEM) in Figure 3c. The dispersion and alignment of graphene in LCEs were further examined by SEM imaging in the charge contrast mode. In the absence of hot drawing, graphene sheets were homogeneously yet disorderly dispersed in the LCE matrix (Figure 3b). In stark contrast, Figure 3d shows that well-dispersed graphene sheets in the LCE matrix were oriented along the hot-drawing direction. Previous work has shown that the ordering of CNTs can be induced by the LC alignment under external fields,[33] and, on the other hand, CNTs were found to assist the alignment of LCs as well.[34] Moreover, the mechanical drawing can not only lead to the orientation of LC mesogens[35] but also promote the alignment of CNTs in the polymer matrix.[36] Likewise, the synergistic interactions (i.e., mutual alignment between LC mesogens and graphene together with the application of the external hot drawing) facilitate the preferential parallel orientation of LC mesogens and graphene sheets along the stretching direction. Interestingly, due to the uniform dispersion and large surface area of graphene, the fractured surface of LCE nanocomposites, regardless of even being hot drawn, appeared to be covered by the wrinkled graphene sheets (Figure 3b,d). It is not surprising as this observation is originated from the fact that the secondary electron yield is predominately enriched at the location of electrically conductive graphene sheets owing to low charge-transport capacity of the insulating LCE matrix.[24a,c]

The photomechanical response of LCE nanocomposites to the NIR light (λ = 808 nm at the power density of 50 mW cm^{-2}) was measured by dynamic mechanical analyzer (DMA) in a tensile mode (Figure S5, Supporting Information). Under a constant force (18 kPa) preloaded to the bottom clamp, pure LCE sample showed a very little shape response to the NIR irradiation (**Figure 4**a). The incorporation of GO, LRGO and HRGO into the LCE matrix resulted in the reversible contraction and expansion under an on–off switching of NIR light at an interval of 120 s. The maximum actuation strain depends strongly on the sp^2-hybridization and the loading content of graphene as well as the extent of hot drawing (accordingly, the degree of alignment) of LCE nanocomposites. In the absence of hot drawing, the HRGO sheets were found to actuate with a larger contraction peak-strain (17.5%) than that of the LRGO (10.7%) and GO (6.1%) sheets for LCEs at the same amount of loading of GO and graphene (0.2%) (i.e., curves 1, 3, and 4). For HRGO sheets in the LCE matrix, the photoinduced deformation also increased with the increase in the amount of loading

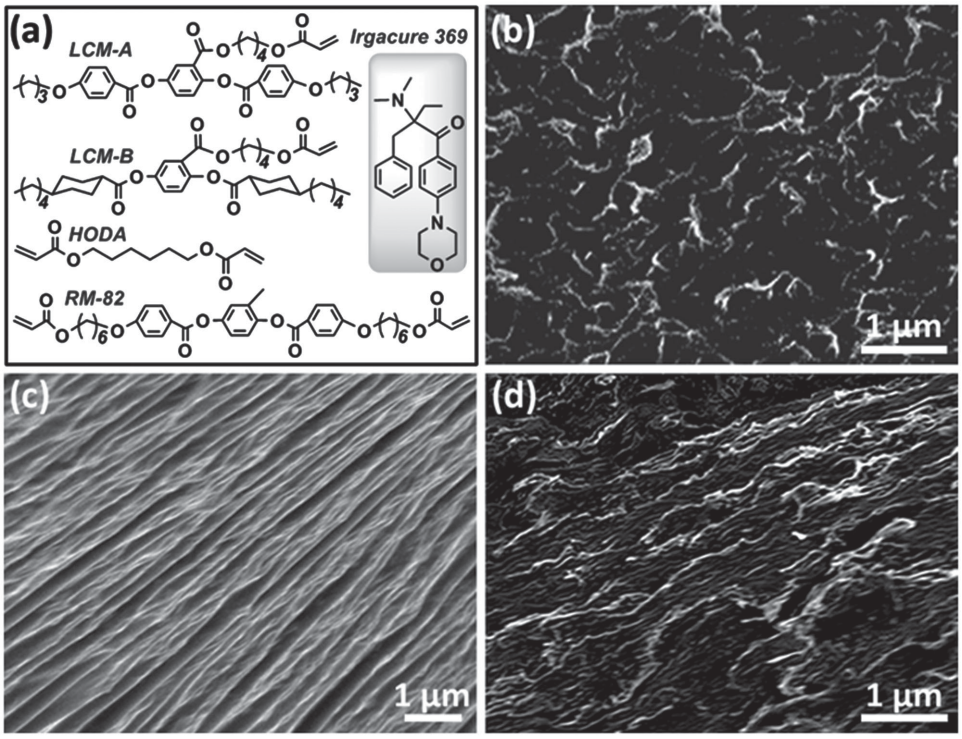

Figure 3. a) Chemical structures of two LCMs (i.e., LCM-A and LCM-B), two cross-linkers of HODA and RM-82, and a photoinitiator of Irgacure 369. SEM images of LCE nanocomposites containing 0.2 wt% HRGO sheets: c) the surface topology (top view) and b,d) the cross-sectional view of freeze-fractured nanocomposites in the charge contrast mode: d) with and b) without the concurrent hot-drawing process.

and the degree of alignment (i.e., curves 2,4,5, and 6). The peak strain for the 0.2% HRGO/LCE nanocomposite without being hot drawn increased from 12.7% (0.1% HRGO/LCE nanocomposite; curve 2) to 17.5% (curve 4), and further rose up to 20.5% after subjecting to the 80% hot drawing (curve 5). Particularly, the photomechanical actuation in the 0.2% HRGO/LCE nanocomposite with a 160% hot drawing started at time $t < 0.5$ s and became saturated at $t \approx 8$ s with a large deformation (35.7%). Subsequently, this nanocomposite underwent a fast relaxation and recovered its original length in less than 8 s upon the switch off of NIR light. We note that the time for achieving the photoactuation saturation is faster than those previously reported in photoresponsive systems, such as the NIR-driven CNT/PDMS (10–15 s),[37] white-light actuated CNT/LCE (≈10 s),[17] and UV–vis light irradiated CNT/LCE (≥50 s)[12] nanocomposites as well as azobenzene-containing LCEs (≥10 s).[38] Moreover, the actuation strains (35.7%) imposed by NIR are comparable to those of CNT/LCE nanocomposites,[17] but significantly larger than CNT/PDMS (2% – 4%)[18b] and graphene/PDMS (≈2% – 5%) nanocomposites.[21]

The exerted force of LCE nanocomposites under NIR irradiation was further examined by subjecting a strip-shaped sample to a constant strain (2%) during the DMA measurement. Figure 4b depicts the actuation stress for pure LCEs and graphene/LCE nanocomposites as a function of the irradiation time. The stress change after being exposed to NIR light exhibited a similar trend as those observed in the actuation strains (Figure 4a). Clearly, comparing to GO- and LRGO-containing nanocomposites (curves 1 and 3, respectively, in Figure 4b) at a 0.2% loading, highly sp^2-hybridized graphene (HRGO) induced a higher actuation stress (curve 4 in Figure 4b) in the absence of hot drawing. It is worth noting that the actuation stress in pure LCE was only ≈20 kPa, similar to those previously reported studies.[30,31b,39] In sharp contrast, the contraction stress was greatly enhanced by incorporating GO and graphene into LCEs and further increased with the increase in the amount of graphene loaded and the degree of alignment of graphene in the LCE matrix. The HRGO/LCE nanocomposites with 160% hot drawing demonstrated a maximum actuation stress of up to 240 kPa, which is close to the contraction force of human muscles (≈300 kPa) yet dramatically higher than that of the CNT/LCE nanocomposites (1.5–8 kPa).[30,31b,39,40]

The long-term NIR response experiments were also conducted to evaluate the stability of the resulting LCE nanocomposites. As shown in Figure 4c, the first three cycles and the 48th–50th cycles of the HRGO/LCE nanocomposite hot drawn to 160% were plotted during a 3.5 h on–off NIR switching at a 2 min interval. Obviously, the contraction peak strains were nearly unchanged, and the photoresponsive sensitivity and reversible stability were well retained over 50 cycles. Such long-term cyclability from photoactuated polymeric materials has been rarely reported previously.

The formation of such intriguing reversible photomechanical actuation in graphene/LCE nanocomposites may be rationalized as follows (Figure 4d). The mechanical extension of graphene/LCE nanocomposites by hot drawing induces the parallel alignment of side-on mesogens and graphene along the stretching direction.[41] When the aligned graphene/

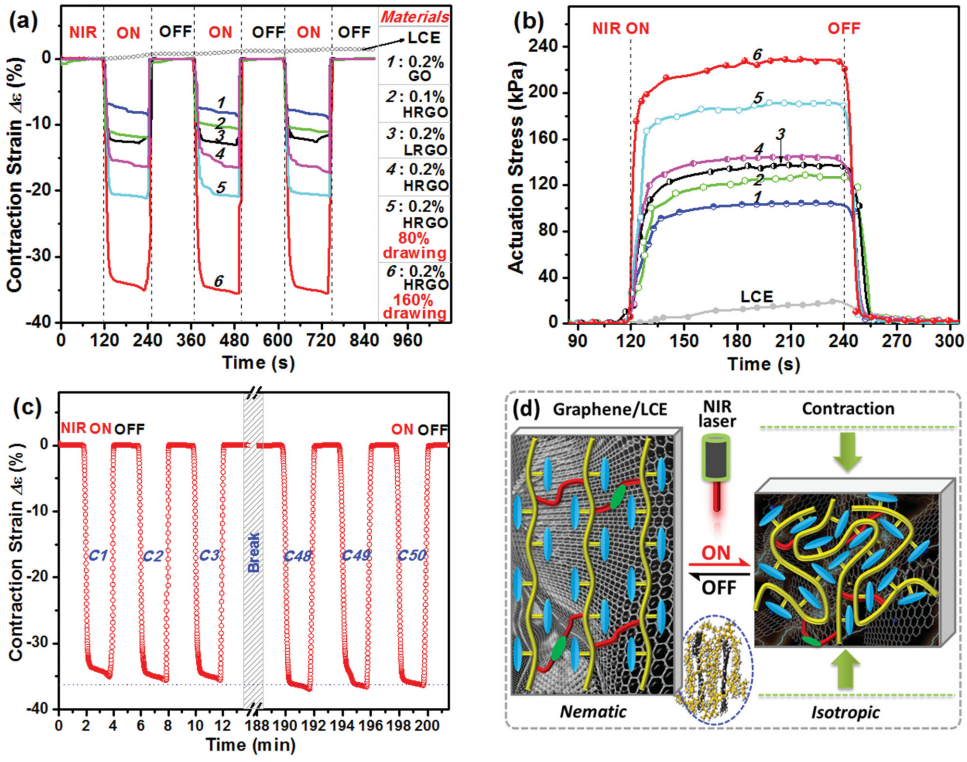

Figure 4. Photomechanical actuation of LCE nanocomposites containing different amount of GO, LRGO, and HRGO sheets and under different degree of hot drawing. a) Contraction strain induced by NIR irradiation under a constant stress (18 kPa). b) Actuation stress generated under a constant strain (2%) and NIR irradiation. c) Long-term cycling responses to NIR irradiation under a constant stress (18 kPa). d) Schematic illustration of reversible photomechanical actuation in graphene/LCE nanocomposites upon an on–off switching of NIR light.

LCE nanocomposites are irradiated by NIR light, the photon energy would be absorbed by graphene surrounded by the LCE matrix and then efficiently converted into thermal energy through phonons in the sp^2-hybridized carbons.[42] Essentially, graphene functions as a nanoscopic heat source and provides a thermally conductive pathway.[18c] Due to the homogeneous dispersion and alignment of graphene, heat generated by continuous NIR irradiation can be uniformly and rapidly propagated throughout the nanocomposite, and thus heats up the LCE matrix and triggers the nematic-to-isotropic phase transition. As evidenced in Figure S6, upon the NIR irradiation on graphene/LCE nanocomposites, their surface temperatures reached a saturation (90–105 °C), which are higher than the T_{NI} of LCE (80–86 °C). This in turn induced a macroscopic contraction under a preload (Figure 4a), and generated an output force under a constant strain (Figure 4b) parallel to the hot-stretching direction. Notably, graphene with more sp^2-bonded carbons exhibits higher intrinsic thermal conductivity and more efficient heat transport via its lattice vibrations,[43] thereby entailing faster response and larger amplitudes of photoactuation in HRGO/LCE as compared to LRGO/LCE nanocomposites.[19b] Conversely, GO sheets with a large fraction of sp^3-bonds possess low amplitudes of photoactuation in the resulting nanocomposite. Moreover, the higher HRGO loading resulted in better actuation performance of nanocomposites due to the presence of more nanoheaters in the LCE matrix. Finally, the hot-drawn LCE nanocomposites comprise the aligned polymer chains and uniformly distributed, ordered graphene sheets, thus markedly enhancing the thermal transfer capability and increasing the amplitude of mechanical actuation unidirectionally.

In summary, we developed, for the first time, graphene-enabled LCE nanocomposites with tunable photomechanical actuation properties via a rational combination of in situ photopolymerization of LCMs in the presence of graphene and concurrent hot-drawing process during the course of photopolymerization. The graphene sheets were homogeneously aligned in the nematic LCE matrix, yielding NIR-responsive nanocomposites with reversible mechanical actuation. Remarkably, large contraction strain, high actuation stress, high initial sensitivity and fast response were simultaneously achieved as a direct consequence of solvothermally enhanced sp^2-hybridization degree of GO and mechanically induced alignment of graphene in LCEs. The actuator performances can be readily tailored by controlling the quality, the loading content, and the degree of alignment of graphene in the LCE matrix. The photoactuation characteristics can also be potentially fine tuned by regulating liquid crystal behaviors of the LCE matrix via internal molecular design (e.g., mesogenic group, spacing group, and crosslinking density) and controlling the external light parameters (e.g., photon energy and irradiation intensity). Such photoactive nanocomposites efficiently integrating the photothermal effect of graphene with the mechanical response of LCEs may open up many possibilities for the exploration of new actuators with tunable functionalities.

Supporting Information

Supporting Information is available from the Wiley Online Library or from the author.

Acknowledgements

The authors thank the financial support from the National Natural Science Foundation of China (51073050 and 51273057), Program for New Century Excellent Talents in University (NCET-12-0709), Key Project of Science and Technology from Ministry of Education of China (210131), Funds for Distinguished Young Scientists of Hubei Province (2015CFA048), and China Scholarship Council (No. 201308420033).

Received: July 29, 2015
Revised: August 17, 2015
Published online: September 21, 2015

[1] a) Z. Pei, Y. Yang, Q. Chen, E. M. Terentjev, Y. Wei, Y. Ji, *Nat. Mater.* **2014**, *13*, 36; b) A. Planes, L. Manosa, *Nat. Mater.* **2014**, *13*, 6; c) Y. Tanaka, Y. Himuro, R. Kainuma, Y. Sutou, T. Omori, K. Ishida, *Science* **2010**, *327*, 1488.

[2] H. Cheng, J. Liu, Y. Zhao, C. Hu, Z. Zhang, N. Chen, L. Jiang, L. Qu, *Angew. Chem. Int. Ed.* **2013**, *52*, 10482.

[3] J. Foroughi, G. M. Spinks, G. G. Wallace, J. Oh, M. E. Kozlov, S. Fang, T. Mirfakhrai, J. D. W. Madden, M. K. Shin, S. J. Kim, R. H. Baughman, *Science* **2011**, *334*, 494.

[4] I. I. Smalyukh, Y. Lansac, N. A. Clark, R. P. Trivedi, *Nat. Mater.* **2010**, *9*, 139.

[5] X. Zhang, Z. Yu, C. Wang, D. Zarrouk, J.-W. T. Seo, J. C. Cheng, A. D. Buchan, K. Takei, Y. Zhao, J. W. Ager, J. Zhang, M. Hettick, M. C. Hersam, A. P. Pisano, R. S. Fearing, A. Javey, *Nat. Commun.* **2014**, *5*, 2983.

[6] A. Sánchez-Ferrer, T. Fischl, M. Stubenrauch, A. Albrecht, H. Wurmus, M. Hoffmann, H. Finkelmann, *Adv. Mater.* **2011**, *23*, 4526.

[7] W. Yuan, L. B. Hu, Z. B. Yu, T. Lam, J. Biggs, S. M. Ha, D. J. Xi, B. Chen, M. K. Senesky, G. Grüner, Q. Pei, *Adv. Mater.* **2008**, *20*, 621.

[8] a) H. Jiang, C. Li, X. Huang, *Nanoscale* **2013**, *5*, 5225; b) J. Naciri, A. Srinivasan, H. Jeon, N. Nikolov, P. Keller, B. R. Ratna, *Macromolecules* **2003**, *36*, 8499.

[9] A. Lendlein, R. Langer, *Science* **2002**, *296*, 1673.

[10] a) A. Lendlein, H. Jiang, O. Junger, R. Langer, *Nature* **2005**, *434*, 879; b) C. L. van Oosten, C. W. M. Bastiaansen, D. J. Broer, *Nat. Mater.* **2009**, *8*, 677.

[11] T. Ikeda, J. Mamiya, Y. L. Yu, *Angew. Chem. Int. Ed.* **2007**, *46*, 506.

[12] W. Wang, X. Sun, W. Wu, H. Peng, Y. Yu, *Angew. Chem. Int. Ed.* **2012**, *51*, 4644.

[13] Y. Yu, M. Nakano, T. Ikeda, *Nature* **2003**, *425*, 145.

[14] a) M. A. Hamon, M. E. Itkis, S. Niyogi, T. Alvaraez, C. Kuper, M. Menon, R. C. Haddon, *J. Am. Chem. Soc.* **2001**, *123*, 11292; b) P. W. Barone, S. Baik, D. A. Heller, M. S. Strano, *Nat. Mater.* **2005**, *4*, 86.

[15] T.-T. Tang, Y. Zhang, C.-H. Park, B. Geng, C. Girit, Z. Hao, M. C. Martin, A. Zettl, M. F. Crommie, S. G. Louie, Y. R. Shen, F. Wang, *Nat. Nanotechnol.* **2010**, *5*, 32.

[16] a) S.-H. Hu, R.-H. Fang, Y.-W. Chen, B.-J. Liao, I. W. Chen, S.-Y. Chen, *Adv. Funct. Mater.* **2014**, *24*, 4144; b) Y. Zeng, J. Q. Lu, *ACS Nano* **2014**, *8*, 11695; c) Y. H. Hu, *Small* **2014**, *10*, 1451.

[17] C. Li, Y. Liu, C.-W. Lo, H. Jiang, *Soft Matter* **2011**, *7*, 7511.

[18] a) H. Koerner, G. Price, N. A. Pearce, M. Alexander, R. A. Vaia, *Nat. Mater.* **2004**, *3*, 115; b) S. V. Ahir, E. M. Terentjev, *Nat. Mater.* **2005**, *4*, 491; c) L. Yang, K. Setyowati, A. Li, S. Gong, J. Chen, *Adv. Mater.* **2008**, *20*, 2271; d) X. Sun, W. Wang, L. Qiu, W. Guo, Y. Yu, H. Peng, *Angew. Chem. Int. Ed.* **2012**, *51*, 8520.

[19] a) J. Liang, Y. Xu, Y. Huang, L. Zhang, Y. Wang, Y. Ma, F. Li, T. Guo, Y. Chen, *J. Phys. Chem. C* **2009**, *113*, 9921; b) J. Loomis, X. Fan, F. Khosravi, P. Xu, M. Fletcher, R. W. Cohn, B. Panchapakesan, *Sci. Rep.* **2013**, *3*, 1900; c) Y. Zhao, L. Song, Z. Zhang, L. Qu, *Energy Environ. Sci.* **2013**, *6*, 3520.

[20] a) W. Jiang, D. Niu, H. Liu, C. Wang, T. Zhao, L. Yin, Y. Shi, B. Chen, Y. Ding, B. Lu, *Adv. Funct. Mater.* **2014**, *24*, 7598; b) C. Wu, J. Feng, L. Peng, Y. Ni, H. Liang, L. He, Y. Xie, *J. Mater. Chem.* **2011**, *21*, 18584; c) E. Wang, M. S. Desai, S.-W. Lee, *Nano Lett.* **2013**, *13*, 2826.

[21] J. Loomis, B. King, T. Burkhead, P. Xu, N. Bessler, E. Terentjev, B. Panchapakesan, *Nanotechnology* **2012**, *23*, 045501.

[22] a) J. Loomis, B. King, B. Panchapakesan, *Appl. Phys. Lett.* **2012**, *100*, 073108; b) J. Loomis, B. Panchapakesan, *Nanotechnology* **2012**, *23*, 215501.

[23] S. V. Ahir, Y. Y. Huang, E. M. Terentjev, *Polymer* **2008**, *49*, 3841.

[24] a) Y. Yang, C.-E. He, W. Tang, C. P. Tsui, D. Shi, Z. Sun, T. Jiang, X. Xie, *J. Mater. Chem. A* **2014**, *2*, 20038; b) Y. Yang, L.-J. Yu, R.-G. Peng, Y.-L. Huang, C.-E. He, H.-Y. Liu, X.-B. Wang, X.-L. Xie, Y.-W. Mai, *Nanotechnology* **2012**, *23*, 225701; c) S. Stankovich, D. A. Dikin, G. H. B. Dommett, K. M. Kohlhaas, E. J. Zimney, E. A. Stach, R. D. Piner, S. T. Nguyen, R. S. Ruoff, *Nature* **2006**, *442*, 282.

[25] C. Ohm, M. Brehmer, R. Zentel, *Adv. Mater.* **2010**, *22*, 3366.

[26] Y. Yang, C.-E. He, R.-G. Peng, A. Baji, X. Du, Y.-L. Huang, X. Xie, Y.-W. Mai, *J. Mater. Chem.* **2012**, *22*, 5666.

[27] a) W. Gao, L. B. Alemany, L. J. Ci, P. M. Ajayan, *Nat. Chem.* **2009**, *1*, 403; b) V. C. Tung, M. J. Allen, Y. Yang, R. B. Kaner, *Nat. Nanotechnol.* **2009**, *4*, 25.

[28] O. C. Compton, B. Jain, D. A. Dikin, A. Abouimrane, K. Amine, S. T. Nguyen, *ACS Nano* **2011**, *5*, 4380.

[29] S. Dubin, S. Gilje, K. Wang, V. C. Tung, K. Cha, A. S. Hall, J. Farrar, R. Varshneya, Y. Yang, R. B. Kaner, *ACS Nano* **2010**, *4*, 3845.

[30] Y. Ji, Y. Y. Huang, R. Rungsawang, E. M. Terentjev, *Adv. Mater.* **2010**, *22*, 3436.

[31] a) C. Li, Y. Liu, X. Huang, H. Jiang, *Adv. Funct. Mater.* **2012**, *22*, 5166; b) J. E. Marshall, Y. Ji, N. Torras, K. Zinoviev, E. M. Terentjev, *Soft Matter* **2012**, *8*, 1570.

[32] D. L. Thomsen, P. Keller, J. Naciri, R. Pink, H. Jeon, D. Shenoy, B. R. Ratna, *Macromolecules* **2001**, *34*, 5868.

[33] a) M. D. Lynch, D. L. Patrick, *Nano Lett.* **2002**, *2*, 1197; b) C. Zamora-Ledezma, C. Blanc, M. Maugey, C. Zakri, P. Poulin, E. Anglaret, *Nano Lett.* **2008**, *8*, 4103; c) I. Dierking, G. Scalia, P. Morales, D. LeClere, *Adv. Mater.* **2004**, *16*, 865.

[34] R. A. Mrozek, T. A. Taton, *Chem. Mater.* **2005**, *17*, 3384.

[35] Y. Zhao, P. Roche, G. X. Yuan, *Macromolecules* **1996**, *29*, 4619.

[36] X. Xie, Y. Mai, X. Zhou, *Mater. Sci. Eng., R* **2005**, *49*, 89.

[37] S. V. Ahir, E. M. Terentjev, *Phys. Rev. Lett.* **2006**, *96*, 133902.

[38] H. Yu, T. Ikeda, *Adv. Mater.* **2011**, *23*, 2149.

[39] C. J. Camargo, H. Campanella, J. E. Marshall, N. Torras, K. Zinoviev, E. M. Terentjev, J. Esteve, *Macromol. Rapid Commun.* **2011**, *32*, 1953.

[40] N. Torras, K. E. Zinoviev, C. J. Camargo, E. M. Campo, H. Campanella, J. Esteve, J. E. Marshall, E. M. Terentjev, M. Omastová, I. Krupa, P. Teplický, B. Mamojka, P. Bruns, B. Roeder, M. Vallribera, R. Malet, S. Zuffanelli, V. Soler, J. Roig, N. Walker, D. Wenn, F. Vossen, F. M. H. Crompvoets, *Sens. Actuators, A* **2014**, *208*, 104.

[41] a) T. H. Ware, M. E. McConney, J. J. Wie, V. P. Tondiglia, T. J. White, *Science* **2015**, *347*, 982; b) T. Ware, T. White, *Polym. Chem.* **2015**, *6*, 4835.

[42] A. A. Balandin, *Nat. Mater.* **2011**, *10*, 569.

[43] H. Zhang, A. F. Fonseca, K. Cho, *J. Phys. Chem. C* **2013**, *118*, 1436.